Molecular Theory of Chemically Modified Electrodes by Redox Polyelectrolytes under Equilibrium Conditions: Comparison with Experiment

Mario Tagliazucchi,[†] Ernesto J. Calvo,*[,†] and Igal Szleifer*[,‡]

Molecular Electrochemistry Group. INQUIMAE, DQIAyQF, Facultad de Ciencias Exactas y Naturales. Universidad de Buenos Aires, 1428 Buenos Aires, Argentina, and Department of Chemistry, Purdue University, West Lafayette, Indiana 47907

Received: April 23, 2007; In Final Form: June 6, 2007

A molecular theory is presented to describe chemically modified electrodes by redox polymers. The theory is based on writing the free energy functional of the system which includes the size, shape, charge distribution, and conformations of all of the molecular species as well as all of the inter and intramolecular interactions, the acid−base equilibrium for the ionizable groups of the weak polyelectrolyte, and the redox equilibrium of the electrochemical active sites with the metal. The minimization of the free energy leads to the molecular organization of the film as a function of bulk pH, salt concentration, and applied electrode potential. The approach is applied to the experimental system composed by osmium pyridine−bipyridine complex covalently bound to poly(allylamine) backbone, which is adsorbed onto a mercapto-propane sulfonate thiolated gold electrode. The redox and nonredox capacity of the electrode and its dependence on the electrode potential calculated with the molecular theory shows very good agreement with linear scan voltammetric experiments under reversible conditions (equilibrium scans) without the use of any free adjustable parameter. The predicted film thickness is in line with ellipsometric measurements. Further, the theory predicts the swelling of the film as a function of the electrode potential. The molecular theory provides the link between the molecular organization within the film and the electrochemical behavior. It is shown that the electrostatic, excluded volume, and van der Waals interaction fields are strongly coupled in a nontrivial way. Furthermore, the degree of charge regulation and distribution of oxidized states couples to the molecular distributions and the interaction fields. The application of the theory to different model systems demonstrates the importance of incorporating molecular information into the theoretical approach and the very strong coupling that exists between molecular structure, film organization, interactions fields, and electrochemical behavior.

1. Introduction

Since the first demonstration of a chemically grafted group to a platinum electrode surface,[1] chemically modified electrodes by single and multiple molecular layers have been extensively studied.[2−4] These integrated chemical systems[5] have found applications in chemical sensors, electrocatalysis, molecular electronics, electrosynthesis, energy conversion, and as molecular wires in amperometric enzyme electrodes.[6]

Polymer-modified electrodes, built up by deposition of electroactive polymeric films on conductive substrates, have been a major area of research for the last three decades.[7,8] Despite the intense experimental activity in the area, much of the theoretical work relies on phenomenological ideas, due to the molecular complexity of the problem.[7] Examples are the Donnan partition model[9] originally introduced by Anson and Redepending[10,11] to study the formal redox potential dependence on ionic strength; the Laviron[12] model that takes account of lateral interactions which determine the peak position, shape, and width in cyclic voltamperograms; and the insights on charge and mass transport within polymer film electrodes developed by Seveant and Andriuax[13−16] and Laviron.[17] There is also the microscopic model of Chidsey and Murray[18] based on a cubic lattice with site interactions and the chemical and mechanical description of polymer-modified electrodes of Bowden et. al.[19−21] Even though the usefulness of these simple approaches is not under discussion, they provide only a partial description of the electrochemical process and do not include specific molecular characteristics of the film. For example, the conformational degrees of freedom of polymer chains, the shape and size of the molecules, the local activity coefficients of the electroactive species, the properties of the underlying substrate, and the existence of coupled acid base equilibria have been neglected in those simplified treatments. For instance, despite the extensive literature in polymer modified electrodes, only recent models from Posadas et al.[22] and Lizarraga et al.[23] have included some statistical description of polymer chains, based on the Flory theories for polymer free energy of mixing and elastic deformation.[24]

There are extensive theoretical studies on the structure and properties of adsorbed polyelectrolytes. The methods that have been applied include mean-field, scaling, self-consistent field and molecular theories. For an extensive review, see ref 25 and references therein. However, to the best of our knowledge, there are no theoretical studies treating the link between the electrochemical properties of redox-polymer modified electrodes with the layer's molecular organization. The aim of the work presented here is to provide such an approach.

* Corresponding authors: (E.J.C.) e-mail: calvo@qi.fcen.uba.ar; (I.S.) permanent address: Department of Biomedical Engineering, Northwestern University, 2145 Sheridan Rd., Evanston, IL. E-mail: igalsz@northwestern.edu.
[†] Universidad de Buenos Aires.
[‡] Purdue University.

10.1021/jp073123f CCC: $37.00 © xxxx American Chemical Society
Published on Web 08/30/2007 PAGE EST: 13.7

CHART 1: PAH-Os Chemical Structure

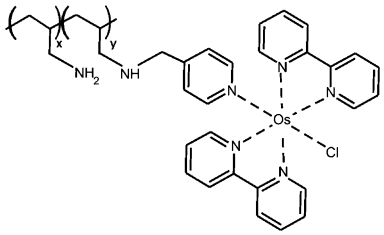

In the present work, we present for the first time a molecular theory for the complete description of reversible electrochemical processes in polymer film-coated electrodes. Namely, we study the equilibrium behavior of the polymer modified electrodes. The general theory will be applied to the particular case of a single layer of poly(allylamine) derivatized with the osmium complex $Os(bpy)_2ClPy^{+/2+}$ covalently attached to the polymer backbone (PAH-Os, see Chart 1), adsorbed on a mercaptopropane sulfonate (MPS) modified Au electrode. This redox polyelectrolyte has been extensively studied as a molecular wire in layer by layer self-assembled systems[26,27] such as enzymatic biosensors,[28−32] and it is a model system of polymer modified electrodes.

In this first report, a comparison of the molecular theory predictions with experimental results of cyclic voltammetry (CV) and ellipsometry under reversible conditions for the redox polyelectrolyte modified electrode Au/MPS/(PAH-Os) will be presented.[33] The theory predicts the molecular organization of the film as a function of the electrode potential and solution composition. By the molecular organization, we refer to the concentration profiles of all molecular species, including acid−base equilibrium of the weak polyelectrolyte, the electrostatic potential profile, the conformations of the polymers, and the distribution of redox sites and oxidation states.

The paper is organized in the following way: We present the derivation of the theory followed by the molecular model for PAH-Os. Section 4 describes the experimental studies. Section 5 presents the comparison of the theoretical predictions and experimental observations together with the molecular structure of the film and its changes upon variation of the experimental variables. The last section discusses some concluding remarks and directions for future work.

2. Theoretical Approach

We have based our theoretical approach on the molecular theory (MT)[34−37] which has been widely used to investigate the properties of non-redox-grafted polymer and polyelectrolyte layers. The MT explicitly incorporates the size, shape, conformations, charge, and charge distribution of all molecular species. The theory is a density functional approach in which the interaction fields are determined in a self-consistent fashion by considering very detailed models for each of the molecular components of the system. We obtain detailed structural information of the film as well as the thermodynamic properties. In particular, as it will be shown in the results section, we demonstrate the strong coupling that exists between the thermodynamic state and the structure of the system. In this way we study how variations in solution conditions, e.g., ionic strength and pH among others, and the electrode potential changes the structure of the film as well as the thermodynamic properties.

The theory is derived by writing the free energy of the system as a functional of the densities of the species in solution, the conformations of the polymer and the electrostatic potential, explicitly considering the acid−base and redox equilibria. We will provide a detailed derivation below of the theory with special emphasis on the novel application to include redox groups as well as the equilibrium with an electrode. For a detailed derivation of the theory with a long discussion of its advantages and limitations, the reader is referred to refs 34−36.

The PAH-Os modified electrode is schematically drawn in Figure 1. The cartoon includes all of the chemical reactions considered by the theory. The polyelectrolyte film is deposited on a thiolated gold surface, which acts both as an electrode and as a support to anchor the redox polymer. The z axis is considered to be perpendicular to the electrode, and its origin ($z = 0$) is located at the surface of the metal. For simplicity, we shall consider only inhomogeneities in the direction perpendicular to the surface. The generalization to treating inhomogeneous systems in all three dimensions has been demonstrated elsewhere.[36] It is important to emphasize that considering inhomogeneities only in the z direction does not imply that we are not treating the lateral interactions. Rather, it implies that for each distance z from the electrode, the $x-y$ plane is homogeneous; that is, the lateral interactions at each z are treated within a mean-field approximation. This approximation is very good, as it has been shown by comparisons of the predictions of the theory with experimental observations for the structure of poly(acrylic acid) layers as a function of pH and solution ionic strength[37] and in the adsorption of proteins on surfaces modified with uncharged polymers.[38,39] Therefore, we are confident that this approximation is well suited to the polymer modified electrodes treated in this work. This assumption will be confirmed by the very good agreement that we find between the experimental observations and the predictions of the theory (see, e.g., Figures 2 and 3 below).

In our treatment, the polymer is described in terms of its two parts: the polymeric backbone and the tethered redox sites. The polymer backbone is composed of segments representing the allyl-amine units; each one bears a protonable amino group, and the volume of the segment is represented by υ_p. The redox sites represent the pyridine−bipyridine osmium complex, which could be in the oxidized Os(III) or in the reduced Os(II) state. The redox sites are attached to the polymer backbone and modeled as spherical units of radius r_{Os} and volume υ_{Os}. The modified electrode is immersed in an aqueous electrolyte solution containing salt ions at concentration C_{salt} and protons and hydroxyls ions at concentration given by the bulk solution pH.

The derivation of the theory is based on writing the total free energy of the system. We will next describe each contribution to the free energy in detail, followed by the expressions used to determine the equilibrium electrochemistry that is compared with the experimental observations. We consider N_P chains of PAH-Os and N_{MPS} chains of MPS adsorbed over an electrode of area A (see Figure 1). The total Helmholtz free energy for this system can be written as

$$F = -TS_{w,mix} - TS_{A,mix} - TS_{C,mix} - TS_{H^+,mix} - TS_{OH^-,mix} - TS_{pol} - TS_{MPS} - TS_{NH_2/NH_3^+} - TS_{SO_3^-/HSO_3} - TS_{Os(III)/Os(II)} + F_{e^-} + F_{vdW} + F_{Elec} + F_{P-S} + F_0 \quad (1)$$

For practical purposes it is convenient to use the free energy density, free energy per unit area $\beta F/A$, with $\beta = (k_B T)^{-1}$. We now express each of the terms in the free energy density, eq 1, as functionals of the corresponding densities and distribution probabilities.

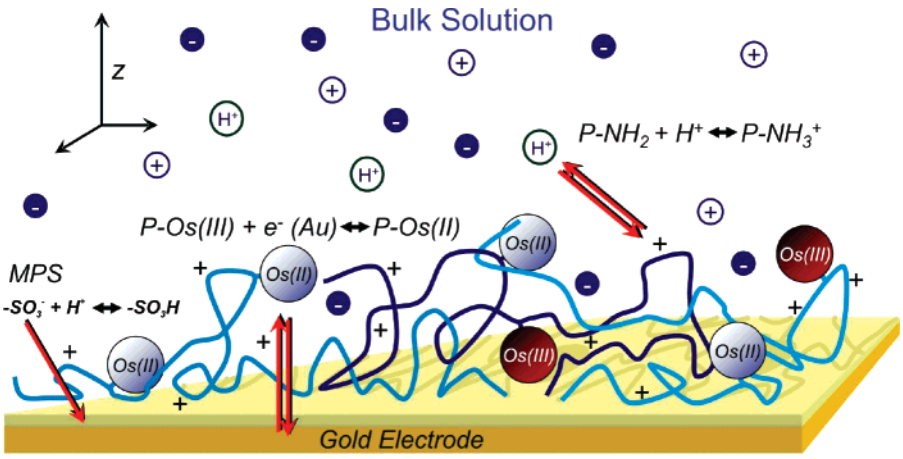

Figure 1. Schematic representation of the Au/MPS/PAH-Os/solution interface. The red arrows indicate the chemical equilibria considered by the theory. The redox polymer, PAH-Os (see Chart 1), is divided into the poly(allyl-amine) backbone (depicted as blue and light blue solid lines) and the pyridine-bipyridine osmium complexes. Each osmium complex is in redox equilibrium with the gold substrate and, depending on its potential, can be in an oxidized Os(III) (red spheres) or in a reduced Os(II) (blue sphere) state. The allyl-amine units can be in a positively charged protonated state (plus signs on the polymer backbone lines) or in a neutral deprotonated state, which are related by an acid−base equilibrium. The self-assembled layer of a mercapto-propane sulfonate, MPS, is covalently adsorbed on top of the gold substrate (depicted as a yellow layer covering the electrode). The sulfonate groups in MPS are in acid−base equilibrium with protons in solution and thus could be in a protonated or in a deprotonated state. The polymer-modified electrode is immersed in an aqueous electrolyte solution containing salt ions, protons, and hydroxyls in thermodynamic equilibrium which a bulk solution. The normal direction from the electrode is denoted by z and has its origin on the metal surface.

The first five terms in eq 1 are the z-dependent translational (mixing) entropies for the mobile species

$$\frac{S_{i,\mathrm{mix}}}{Ak_\mathrm{B}} = -\int \rho_i(z)[\ln(\rho_i(z)\upsilon_\mathrm{w}) - 1]\,\mathrm{d}z \tag{2}$$

where υ_w is the volume of the solvent (water), used as the volume unit throughout. ρ_i (z), i = w, H^+, OH^-, C, A, is the number density of water molecules, proton, hydroxyls, cations, and anions, respectively. The sixth term in eq 1 is the conformational entropy of the polymer chains given by

$$\frac{S_\mathrm{pol}}{Ak_\mathrm{B}} = -\frac{N_\mathrm{P}}{A}[\sum_\alpha P_\mathrm{P}(\alpha)\ln P_\mathrm{P}(\alpha)] \tag{3}$$

where $P_\mathrm{P}(\alpha)$ is the probability of having a chain in the conformation α. The conformation refers to the positions of each of the segments and the redox sites; that is, each conformation represents a particular volume distribution of the allyl-amine segments and osmium complexes in space.

The entropy of the thiol is described with a similar expression

$$\frac{S_\mathrm{MPS}}{Ak_\mathrm{B}} = -\frac{N_\mathrm{MPS}}{A}[\sum_\gamma P_\mathrm{MPS}(\gamma)\ln P_\mathrm{MPS}(\gamma)] \tag{4}$$

with $P_\mathrm{MPS}(\gamma)$ representing the probability of having the thiol chain in conformation γ.

The amino groups in the polymer and the sulfonate groups in the thiol may exist in two different states (protonated or deprotonated), related by an acid−base chemical equilibrium. The existence of more than one possible chemical state for a given chemical moiety introduces a z-dependent entropic mixing contribution to the free energy of the two species. More specifically

$$\frac{S_{\mathrm{NH_2/NH_3^+}}}{Ak_\mathrm{B}} = -\int\langle n_\mathrm{P}(z)\rangle[f_\mathrm{c}(z)\ln(f_\mathrm{c}(z)) + (1-f_\mathrm{c}(z))\ln(1-f_\mathrm{c}(z))\,\mathrm{d}z \tag{5}$$

and

$$\frac{S_{\mathrm{SO_3^-/HSO_3}}}{Ak_\mathrm{B}} = -\int\langle n_\mathrm{MPS}(z)\rangle[f_\mathrm{c,MPS}(z)\ln(f_\mathrm{c,MPS}(z)) + (1-f_\mathrm{c,MPS}(z))\ln(1-f_\mathrm{c,MPS}(z))\,\mathrm{d}z \tag{6}$$

In these equations $f_\mathrm{c}(z)$ ($f_\mathrm{c,MPS}(z)$) is the fraction of the amino (sulfonate) groups at z that are charged. The average densities of polymer (thiol) segments at a distance z from the surface are denoted as $\langle n_\mathrm{P}(z)\rangle$ ($\langle n_\mathrm{MPS}(z)\rangle$). In the case of the polymer, $\langle n_\mathrm{P}(z)\rangle$ is calculated as

$$\langle n_\mathrm{P}(z)\rangle = \frac{N_\mathrm{P}}{A}\sum_\alpha P_\mathrm{P}(\alpha)\,n_\mathrm{P}(z,\alpha) \tag{7}$$

where $n_\mathrm{P}(z,\alpha)$ is the number of polymer allyl-amine segments that a chain in conformation α has at z. A similar expression holds for the thiol.

The redox sites could also exist in two different oxidation states related by the redox equilibrium. The corresponding entropy of mixing for the two chemical states is

$$\frac{S_\mathrm{Os(III)/Os(II)}}{Ak_\mathrm{B}} = -\int\langle n_\mathrm{Os}(z)\rangle[f_\mathrm{Os}(z)\ln(f_\mathrm{Os}(z)) + (1-f_\mathrm{Os}(z))\ln(1-f_\mathrm{Os}(z))\,\mathrm{d}z \tag{8}$$

where $f_\mathrm{Os}(z)$ is the fraction of oxidized sites at z and $\langle n_\mathrm{Os}(z)\rangle$ is the average density of redox sites at z (see eq 7).

The term F_{e-} in eq 1 is the electrical work necessary to bring the redox sites in the system from a fully oxidized reference state to their final redox state. This process requires the flux of N_{e-} electrons from the vacuum to the system. Since we are dealing with a system in equilibrium

$$\frac{\beta F_{e^-}}{A} = \frac{N_{e^-}}{A}\beta|e|E_\mathrm{eq}^\mathrm{abs} \tag{9}$$

where $E_\mathrm{eq}^\mathrm{abs}$ is the electrode potential of the metal in the absolute scale.[40] The required number of electrons in eq 9, N_{e-},

is calculated from the final number of reduced redox sites in the system

$$\frac{N_{e^-}}{A} = \int \langle n_{Os}(z)\rangle [1 - f_{Os}(z)]\, dz \quad (10)$$

Note that this term couples the potential of the electrode with the oxidation fraction at each distance z from the surface.

F_{vdW} in the free energy expression represents the van der Waals (vdW) interactions. As it is well-known from the polymer literature,[41] this term represents the quality of the solvent and it measures the likeness of the polymer segments for the solvent. In polymer solutions, the quality of the solvent is given by the so-called Flory−Huggins interaction parameter, which is a measure of the relative attractions between the polymer segments as compared to the polymer−solvent interactions.[41,42] This concept was generalized for inhomogeneous environments with the molecular theory, originally to study polymer brushes in poor solvents,[34,43] to lead for the free energy the expression

$$\frac{\beta F_{vdW}}{A} = \int\int \frac{\beta\chi(|z - z'|)}{2}[\langle\phi_{Os}(z)\rangle + \langle\phi_P(z)\rangle][\langle\phi_{Os}(z')\rangle + \langle\phi_P(z')\rangle]\, dz\, dz' \quad (11)$$

Here $\chi(|z - z'|)$ is a distance dependent vdW interaction parameter (generalized Flory−Huggins interaction parameter) that accounts for the non-homogeneous distribution of the polymer segments. $\langle\phi_P(z)\rangle$ and $\langle\phi_{Os}(z)\rangle$ are the polymer backbone and redox site volume fractions respectively, given by

$$\langle\phi_P(z)\rangle = \frac{N_P}{A}\sum_\alpha P_P(\alpha)\, \upsilon_P(z, \alpha) \quad (12)$$

$$\langle\phi_{Os}(z)\rangle = \frac{N_P}{A}\sum_\alpha P_P(\alpha)\, \upsilon_{Os}(z, \alpha) \quad (13)$$

where $\upsilon_P(z, \alpha)$ and $\upsilon_{Os}(z, \alpha)$ are the volume occupied at distance z from the surface by the polymer segments and the redox sites, respectively, when the chain is in conformation α.

The electrostatic contribution to the free energy is given by[36,44,45]

$$\frac{\beta F_{Elec}}{A} = \beta\int\left[\langle\rho_Q(z)\rangle\psi(z) - \frac{1}{2}\epsilon(z)(\nabla_z\psi(z))^2\right] dz \quad (14)$$

where $\psi(z)$ and $\epsilon(z)$ are the z-dependent outer electrostatic potential and dielectric coefficient respectively, and $\langle\rho_Q(z)\rangle$ is the average density of charges at z given by

$$\langle\rho_Q(z)\rangle = \langle n_P(z)\rangle f_c(z) q_{NH_3^+} + \langle n_{Os}(z)\rangle\, [q_{Os(III)} f_{Os}(z) + q_{Os(II)}\,(1 - f_{Os}(z))] + \langle n_{MPS}(z)\rangle f_{c,MPS}(z) q_{MPS} + \rho_A(z) q_A + \rho_C(z) q_C + \rho_{H^+}(z) q_{H^+} + \rho_{OH^-}(z) q_{OH^-} \quad (15)$$

which includes contributions from the poly(ally amine) backbone, the redox sites, the thiol molecules, salt anions and cations, protons and hydroxyl ions respectively. In this equation, q_i is the charge of the specie i in units of the elemental charge.

F_{P-S} in eq 1 represents the vdW interaction between the polymer and the thiolated layer; that is, it can be thought as the polymer adsorption energy, and it is given by

$$\frac{\beta F_{P-S}}{A} = \frac{N_P}{A}[\sum_\alpha P_P(\alpha)\beta U_{PS}(\alpha)] \quad (16)$$

where the interactions between the polymer and the thiol are modeled by a square well potential and thus

$$U_{ps} = \int_0^{\delta_P} \epsilon_{P-S}\langle n_P(z)\rangle\, dz + \int_0^{\delta_{Os}} \epsilon_{Os-S}\langle n_{Os}(z)\rangle\, dz \quad (17)$$

where ϵ_{P-S} (ϵ_{Os-S}) is the strength of the segment-surface (redox site-surface) interactions and δ_P (δ_{Os}) is the interaction range.

The last term in the free energy, eq 1, includes the standard chemical potentials for the species in the system, μ_i^0

$$\frac{\beta F_0}{A} = \int\langle n_P(z)\rangle(f_c(z)\beta\mu^0_{NH_3^+} + (1 - f_c(z))\beta\mu^0_{NH_2})\, dz + \int\langle n_{MPS}(z)\rangle(f_{c,MPS}(z)\beta\mu^0_{SO_3^-} + (1 - f_{c,MPS}(z))\beta\mu^0_{HSO_3})\, dz + \int\langle n_{Os}(z)\rangle(f_{Os}(z)\beta\mu^0_{Os(III)} + (1 - f_{Os}(z))\beta\mu^0_{Os(II)})\, dz + \int\mu^0_{H^+}\rho_{H^+}(z)\, dz + \int\mu^0_{OH^-}\rho_{OH^-}(z)\, dz \quad (18)$$

In eq 18, we have included only the standard chemical potentials of the species that participate in chemical equilibria, since the others have no thermodynamic consequences. We should mention that all of the chemical potentials and standard chemical potentials in the theory include the electrostatic contribution and therefore correspond to the electrochemical potentials used in the electrochemical literature.[8]

The repulsive interactions between all molecular species are not explicitly included in the free energy expression, eq 1. We model them as excluded volume interactions. They are included in the theory in the generation of the chains, which are all self-avoiding (see the Supporting Information) and as packing constraints for the intermolecular repulsions. Namely, the sum of the volume that each of the species occupies at z should be equal to the total available volume at z. This leads to

$$\sum_i \phi_i(z) = 1 \quad (19)$$

for all z, where $\phi_i(z)$ is the volume fraction for the species i at z. For solvent (water), protons, hydroxyls ions, cations, and anions (i = w, H^+, OH^-, C, and A), $\phi_i(z)$ is equal to $\rho_i(z)\upsilon_i$, where υ_i is the molecular volume of the species i. For polymer segments, redox sites, and MPS molecules, it is equal to the average volume fractions $\langle\phi_i(z)\rangle$ (i = P, Os, and MPS) as defined by eqs 12 and 13.

We require the global electroneutrality of the system. Therefore, we impose the following constraint to the free energy

$$\int\langle\rho_Q(z)\rangle\, dz + \sigma_M = 0 \quad (20)$$

where σ_M is the charge on the metal and the integral includes all of the charges in the system up to, and including, the bulk solution. The distribution of the charged species as a function of the distance from the surface is an important output of the theory, and as it will be shown, it depends on the experimental conditions.

The polymer-modified electrode is in equilibrium with a bulk solution. Therefore, at thermodynamic equilibrium, the chemical potential of all of the free species in the solution should be the same at all z. Note that this condition does not apply to the polymer and the thiol since they are attached to the surface. Namely, we are treating the polymer layer under the assumption that the total number of adsorbed polymers is known and fixed. Thus, we need to consider a semi-grand-canonical potential, W, which is canonical for polymer and thiol and grand canonical for the other species. Writing explicitly the packing and

electroneutrality constraints to the free energy and including the chemical equilibrium with the bulk solution through the chemical potentials leads to

$$\frac{\beta W}{A} = \frac{\beta F}{A} + \int \beta\pi(z)[\sum_i \phi_i(z) - 1]\, dz + \lambda \int \langle \rho_Q(z) \rangle\, dz - \beta\mu_C \int \rho_C(z)\, dz - \beta\mu_A \int \rho_A(z)\, dz \quad (21)$$

with λ and $\pi(z)$ being the Lagrange multipliers associated with the electroneutrality and packing constraints respectively. As was explained in ref 36, the chemical potentials of protons, hydroxyls ions, and solvent molecules do not appear explicitly in this equation because the presence of constraints (charge neutrality and packing constraint) reduces the number of independent thermodynamic variables by three.

The extremum of the semi-grand-potential functional with respect to $\rho_i(z)$, $f_c(z)$, $f_{Os}(z)$, $f_{c,MPS}(z)$, $\psi(z)$, and $P(\alpha)$ provides for explicit expressions for the volume fraction of the free species, the probability distribution functions of the polymer, and the z-dependent chemical equilibria.

The variation with respect to $P(\alpha)$ leads to the probability distribution function (PDF) for the polymer chains

$$P_p(\alpha) = \frac{1}{\xi} \exp\Bigg\{ -\int n_p(z, \alpha)[\ln(f_c(z)) + q_{NH_3^+}(\beta\psi(z) + \lambda) + \beta\mu^0_{NH_3^+}]\, dz - \int n_{Os}(z, \alpha)[q_{Os(II)}(\beta\psi(z) + \lambda) + \ln(1 - f_{Os}(z)) + \beta\mu^0_{Os(II)}]\, dz - \beta U_{PS}(\alpha) - \int [\upsilon_p(z, \alpha) + \upsilon_{Os}(z, \alpha)] \Bigg[\beta\pi(z) + \int \beta\chi(|z - z'|)(\langle \phi_p(z') \rangle + \langle \phi_{Os}(z') \rangle)\, dz' - \frac{1}{2} \frac{d\epsilon(z)}{d(\langle \phi_p(z) \rangle + \langle \phi_{Os}(z) \rangle)} (\nabla_z \psi(z))^2 \Bigg] dz \Bigg\} \quad (22)$$

Here ξ is the normalization constant which guarantees $\Sigma_\alpha P(\alpha) = 1$. Inspection of eq 22 provides further insight about the Lagrange multipliers: λ, enforcing the electroneutrality condition, is a constant term added to the electrostatic potential and $\pi(z)$, which assures the packing constrain at each z, is a lateral osmotic pressure.[34−36] Note that the standard chemical potentials and λ are constant contributions to the PDF and therefore could be included in ξ.

The probability for a given chain conformation in eq 22 has contributions from several of the chemical equilibria and interactions considered by the theory. Namely, the pdf includes the acid−base equilibrium of the amino groups, the redox equilibrium of the osmium complexes, the vdW interactions, and the electrostatic and packing forces. The later two interactions are determined by the interaction fields $\psi(z)$ and $\pi(z)$. These fields are self-consistently determined from the concentration profiles of all the molecular species in the system. As a consequence, a main characteristic of the present theory is that it considers the coupling between the interactions fields and the fact that they are highly nonlocal.

The variation of eq 21 with respect to $\rho_i(z)$ yields the following general relationships for the density profiles of the anion, cation, proton, hydroxyl and solvent:

$$\rho_A(z)\upsilon_w = \exp[-\upsilon_A\beta\pi(z) + \beta\mu_A - q_A\beta(\psi(z) + \lambda)] \quad (23)$$

$$\rho_C(z)\upsilon_w = \exp[-\upsilon_C\beta\pi(z) + \beta\mu_C - q_C\beta(\psi(z) + \lambda)] \quad (24)$$

$$\rho_{H^+}(z)\upsilon_w = \exp[-\upsilon_{H^+}\beta\pi(z) - \beta\mu^0_{H^+} - q_{H^+}\beta(\psi(z) + \lambda)] \quad (25)$$

$$\rho_{OH^-}(z)\upsilon_w = \exp[-\upsilon_{OH^-}\beta\pi(z) - \beta\mu^0_{OH^-} - q_{OH^-}\beta(\psi(z) + \lambda)] \quad (26)$$

$$\rho_w(z)\upsilon_w = \exp(-\upsilon_w\beta\pi(z)) \quad (27)$$

It is convenient to express these relationships in terms of the experimentally accessible bulk number densities, ρ_i^{bulk}, i.e.

$$\rho_i(z)\upsilon_w = \rho_i^{bulk}\upsilon_w \exp(-\upsilon_i\beta[\pi(z) - \pi^{bulk}] - q_i\beta[\psi(z) - \psi^{bulk}]) \quad (28)$$

$$\rho_w(z)\upsilon_w = \rho_w^{bulk}\upsilon_w \exp(-\upsilon_w\beta[\pi(z) - \pi^{bulk}]) \quad (29)$$

where eq 28 holds for the anions, cations, protons and hydroxyls ions and eq 29 for the solvent (water).

The variation of eq 21 with respect to $f_c(z)$ and $f_{c,MPS}(z)$ yields

$$\ln\left(\frac{f_c(z)}{1 - f_c(z)}\right) = -\beta\mu^0_{OH^-} - \beta\mu^0_{NH_3^+} + \beta\mu^0_{NH_2} - \upsilon_{OH^-}\beta[\pi(z) - \pi^{bulk}] - \ln(\rho_{OH^-}(z)) \quad (30)$$

$$\ln\left(\frac{f_{c,MPS}(z)}{1 - f_{c,MPS}(z)}\right) = -\beta\mu^0_{H^+} - \beta\mu^0_{SO_3^-} + \beta\mu^0_{HSO_3} - \upsilon_{H^+}\beta[\pi(z) - \pi^{bulk}] - \ln(\rho_{H^+}(z)) \quad (31)$$

The fractions of charged species has two contributions, one is the standard reaction free energy $\Delta G^0_c = \mu^0_{OH^-} + \mu^0_{NH_3^+} - \mu^0_{NH_2}$ for the allyl-amine backbone segments, eq 30, and $\Delta G^0_{c,MPS} = \mu^0_{H^+} + \mu^0_{SO_3^-} - \mu^0_{HSO_3}$ for the acid−base equilibrium of the sulfonate end-groups of the thiol, eq 31. The second contribution is related to the different packing of the reactants as compared to the products. This is one more manifestation of the close coupling between chemical equilibrium and the other interactions.

Equations 30 and 31 can be rearranged to obtain the generalized acid−base equilibria equations

$$K^0_b = \exp[-\beta\Delta G^0_c] = \frac{\rho_{OH^-}(z)f_c(z)}{1 - f_c(z)} \exp(\upsilon_{OH^-}\beta[\pi(z) - \pi^{bulk}]) \quad (32)$$

$$K^0_a = \exp[-\beta\Delta G^0_{c,MPS}] = \frac{\rho_{H^+}(z)f_{c,MPS}(z)}{1 - f_{c,MPS}(z)} \exp(\upsilon_{H^+}\beta[\pi(z) - \pi^{bulk}]) \quad (33)$$

Here K^0_b and K^0_a are the thermodynamic equilibrium constants, which can be multiplied by the constant factor N_A/ρ_w^{bulk} (with N_A equal to Avogadro's number) to obtain the commonly used equilibrium constants based on molar bulk concentrations.[36] Note that K^0_b and K^0_a are determined by the ratio of the activities at each z and not of the concentrations.

We will now discuss the expressions obtained upon the free energy minimization for the fraction of oxidized sites, $f_{Os}(z)$

$$\ln\left(\frac{f_{Os}(z)}{1-f_{Os}(z)}\right)=\beta|e|E_{eq}^{abs}-\beta\mu_{Os(III)}^{0}+\beta\mu_{Os(II)}^{0}-\beta(q_{ox}-q_{red})(\psi(z)+\lambda) \quad (34)$$

In analogy with the relationships found between local acid base equilibria and the thermodynamic equilibrium constants, eq 34 is a generalized Nerst equation for the Os(II)/Os(III) couple

$$E_{eq}^{abs}=E_{Os(III)/Os(II)}^{0,abs}+\frac{1}{\beta|e|}\ln\left(\frac{f_{Os}(z)}{1-f_{Os}(z)}\right)+\frac{(q_{ox}-q_{red})}{|e|}(\psi(z)+\lambda) \quad (35)$$

where E_{eq}^{abs} and $E_{Os(II)/Os(III)}^{0,abs}$ are the electrode potential in equilibrium and the standard redox potential for the osmium complex in the absolute potential scale[40,46]

$$E_{Os(III)/Os(II)}^{0,abs}=\left[\frac{\mu_{Os(III)}^{0}-\mu_{Os(II)}^{0}}{|e|}\right] \quad (36)$$

The third term in eq 35 accounts for the local electrostatic activity of the redox sites. Although simple in appearance, the strong coupling between the interaction fields and their nonlocal character make this term dependent on all of the interactions and molecular features considered in the theory. Note that in eq 35 the Lagrange multiplier λ appears as an additive constant to the electrostatic potential.

Finally, the extremum of the semi-grand-potential with respect to $\psi(z)$ provides the Maxwell equation for electrostatics

$$\nabla(\epsilon(z)\nabla\psi(z))=-\langle\rho_{Q}(z)\rangle \quad (37)$$

The boundary conditions for eq 37 are the outer electrostatic potential of the metal, $(\psi^{M}+\lambda)$ and the outer potential of the bulk solution $(\psi^{bulk}+\lambda)$. Since only the difference between these potentials is relevant, we have used $\psi^{bulk}=0$ and $\lambda=0$ and therefore ψ^{M} could be determined from the absolute electrode potential as[40]

$$E_{eq}^{abs}=(\psi^{M}+\lambda)-(\psi^{bulk}+\lambda)+\frac{\Phi_{e^-}^{M}}{|e|}=\psi^{M}+\frac{\Phi_{e^-}^{M}}{|e|} \quad (38)$$

where $\Phi_{e^-}^{M}$ is the work function of the metal. Note that E_{eq}^{abs} and ψ^{M} in eq 38 differ only by a constant.

Equation 37 is a generalized Poisson−Boltzmann (P−B) equation since the charge densities depend on the total potential of mean-force. Namely, although the P−B approach considers the local charge to be only a function of the local electrostatic potential,[47] our molecular theory shows how the local charge depends upon the coupling between all of the interactions and the different chemical equilibria involved, see, e.g., eq 22. The strong influence of all of the interactions, as well as the highly nonlocal character of the coupling between the different fields, is seen by realizing that the right-hand side of eq 37 is obtained by replacing the PDF, eq 22, and the density profiles eqs 23−26 into the total charge expression, eq 15.

In order to apply the theory, we need to solve the coupled packing constrain equation, eq 19, and the generalized P−B equation, eq 37. The procedure to carry out the calculations is found in the Supporting Information and in refs 34−36.

The ability to store charge at the electrode-redox polyelectrolyte interface has two contributions that result in the electrode capacity (capacitance per unit area, e.g., F cm^{-2}).[18]

i. The charge at the metal electrode due to thiol, polyions, mobile ions, and solvent dipoles, characterized by a non-redox capacity, $C_{non-redox}$ which is equivalent to the double layer capacity of an ideally polarizable mercury electrode immersed in an electrolyte solution.

The non-redox capacity is given by

$$C_{non-redox}=\frac{\partial\sigma_{M}}{\partial E_{eq}^{abs}} \quad (39)$$

where σ_{M} is the charge on the metal, determined from

$$\sigma_{M}=-\epsilon(0)\frac{\partial\psi}{\partial z}(0) \quad (40)$$

ii. The charge stored in the electroactive material or redox capacity, C_{redox}. The redox capacity is calculated from the potential dependence of total fraction of oxidized redox sites as

$$C_{redox}=F\frac{\partial\Gamma_{Os(III)}}{\partial E_{eq}^{abs}}=F\frac{\partial\int\langle n_{Os}(z)\rangle f_{Os}(z)\,dz}{\partial E_{eq}^{abs}} \quad (41)$$

where F is the Faraday constant and $\Gamma_{Os(III)}$ is the total number of oxidized redox sites per unit area.

The molecular theory allows the straightforward calculation for the electrode capacity from the excess charge in the metal and the excess redox concentration in the polymer film. In previous theoretical models for polymer modified electrodes, these contributions are calculated independently with different models.[4] The non-redox contribution is usually calculated with a constant double layer capacitance directly determined from the experiment. On the other hand, in the molecular theory, both contributions are coupled and are obtained from the same theoretical framework.

3. PAH-Os Molecular Model

In this section, we define the molecular details of the species that are used in the calculations, namely the molecular size and shape, the strength of the molecular interactions, the equilibrium constants, and the surface coverage of the thiol molecules and the polymer chains. These input parameters constitute the molecular model of the system. The conformation of the chains and how they are generated is explained in the Supporting Information. We will refer to the model described in this section as the PAH-Os molecular model since it incorporates specific molecular details for this redox polymer and it will be compared with the experimental observations. In the results section, we present two other models to demonstrate the importance of the molecular details in the predicted behavior of the polymer modified electrode.

We have considered the thiol molecules within the same theoretical framework as the polymer chains. In practice, the thiol molecules are restricted to the first 0.5 nm from the metal, which is equal to the discretization length (see the Supporting Information). Therefore, in this model, all conformations of the thiol molecule are equivalent, and we can write

$$\langle n_{MPS}(z)\rangle=\begin{cases}\dfrac{\sigma_{MPS}}{0.5\text{ nm}} & 0\text{ nm}<z<0.5\text{ nm}\\ 0 & z>0.5\text{ nm}\end{cases} \quad (42)$$

$$\langle\phi_{MPS}(z)\rangle=\langle n_{MPS}(z)\rangle\nu_{MPS} \quad (43)$$

TABLE 1: Charge and Volume Used in the PAH-Os Molecular Model

	electrostatic charge, q_i	molecular (segment) volume, v_i (Å^3)
water	0	30
cation	+1	33.5
anion	−1	33.5
proton	+1	30
hydroxyl ions	−1	30
polymer segment (allyl-amine)	+ 1 (NH_3^+) 0 (NH_2)[a]	113
thiol molecule	−1 (SO_3^-) 0 (HSO_3)[b]	580
redox site (osmium complex)	+2 (Os^{III}) +1 (Os^{II})	1770

[a] $pK_b = 5$. [b] $pK_a = -1$.

where σ_{MPS} is the surface coverage of the thiol molecules equal to N_{MPS}/A and v_{MPS} is the molecular volume of the thiol molecule (see Table 1). We have employed the experimentally reported MPS surface coverage of 4.6×10^{-10} mol cm^{-2}.[48] Short chain thiols yield disordered films with submonolayers coverages on gold[48] in contrast to the compact monolayers observed for longer thiols.[49] In this model, 80% of the metal surface is covered by thiols, and thus, water and ions permeate into the layer. On the basis of calculations results (not shown) that showed that polymer chains practically do not penetrate the thiol layer, we have not allowed polymer at $z < 0.5$ nm to simplify the calculations.

The high surface density of the thiol molecules motivated the inclusion in the theory of the sulfonate acid−base equilibrium. Even though the sulfonic moieties are strong acids, the highly negative environment in the MPS layer favors the protonation of the sulfonate groups, in a process known as charge regulation.[50] Our calculations (using $pK_a = -1$) indicate that it is necessary to include this effect since the effective charge of the thiols, $f_{c,MPS}$, is highly dependent on the bulk pH, salt concentration, and electrode potential. For example, we find a decrease in the degree of dissociation from 0.96 in a solution with a salt concentration of 0.1 M to 0.82 in a low salt ($C_{salt} = 10^{-3}$ M) solution, where ions are unable to screen MPS charges. The lower degree of charge at low salt concentrations is also predicted to be potential dependent. We find that $f_{c,MPS}$ increases about 7% when increasing the electrode potential in the range studied in sections 5.1 and 5.4.

The PAH-Os chains on top of the thiol are constrained to have at least one segment in 0.5 nm $< z <$ 1.0 nm in order to prevent chain desorption. In the present work, we have not theoretically studied the adsorption of the redox polymer but calculated the polymer surface coverage (2.1 segments/nm^2) from the oxidation charge obtained from CV experiments (2.6 ± 0.2 μC.cm^{-2}) and the ratio of redox sites to polymer segments (1:13) determined from XPS measurements.[51] Although the theory requires as an input all of the possible conformations of the polymer, this is impossible for the chain lengths considered in this work, and therefore, we have used a large representative set of 10^5 conformations (see the Supporting Information for details on chain generation). The experimental polymer chain length (n) of ∼780 allylamine segments is too long for proper generation of independent conformations;[52] thus, we have studied the effect of the chain length in the range of 26−156 segments. Since the electrochemical response was found to became independent of the chain length for $n > 78$ (see the Supporting Information), we decided to describe the experimental polymer chains of 780 segments as 6 independent chains of $n = 130$.

In order to estimate the vdW interaction strengths, we will take advantage of our previous knowledge about PAH-Os. Let us consider the end-to-end distance for free polymer, in the absence of interactions this is equal to $n^{1/2}l$, where n is the chain length and l is the length of a segment.[24] We can use $n = 780$ and $l = 0.5$ to obtain an end to end distance of 14.0 nm, which is very different from the experimental thickness observed for PAH-Os layers of 1−2 nm.[26,53] Based on this observation, hydrophobic polymer−polymer and polymer−thiol interactions must exist in order to constrain the chains to the surface. The existence of hydrophobic polymer−polymer interactions is also supported by the high solubility of totally deprotonated PAH in nonpolar solvents. We model the poor solvent characteristics of the allyl-amine segments using the interaction parameters shown in the Supporting Information which are based on the calculations presented in ref 43. These conditions correspond to an effective temperature for the solvent that is 0.75θ, where θ is the temperature at which the second virial coefficient of the polymer chains vanishes.[42] The polymer-thiolated surface interaction, ϵ_{P-S}, and the redox site-thiolated surface interaction, ϵ_{P-Os}, have been taken as −1.0 and −2.0 kT respectively with an interaction range of 1.0 nm. These values are similar to those usually employed in Monte Carlo[54] and molecular dynamics[55] simulations to describe the adsorption of polymers on flat surfaces.

On the basis of previous work,[36,44] we will assume that the dielectric function, $\epsilon(z)$ is constant in the polymer/solution region. However, the permeable thiol layer has a different value and therefore the model is that of a metal for $z < 0$, $\epsilon(z) = \epsilon_{thiol} = 3.8$ for $0 < z < 0.5$ nm and $\epsilon(z) = \epsilon_w = 78$ for $z > 0.5$ nm.

Using the molecular model described in this section, with parameters found in Table 1, we have solved the nonlinear coupled equations for each condition of interest as described in the Supporting Information.

3. Experimental Section

3.1. Reagents and Materials. All solutions were prepared with 18 MΩ Milli-Q (Millipore) water. Sodium 3-mecapto-propane-sulfonate, MPS (Aldrich) was used as received. The chemicals employed in electrolyte solutions, $NaNO_3$ and HNO_3, were of analytical grade and used without further purification.

The osmium bipyridine derivatized redox polymer $Os(bpy)_2$-$ClPyCH_2NH$-poly(allylamine) (PAH-Os) was synthesized as previously reported[56.] Thiol solutions of 20 mM 3-mercapto-1-propane-sulfonic acid (MPS) (Aldrich) in 10 mM sulfuric acid (Merck) were prepared before each experiment in order to avoid oxidation in air. The PAH-Os solution was adjusted to pH 8.3 employing 0.1 M solutions of HCl or NaOH respectively.

3.2. Surface Modification. Silicon (100) substrates were coated with a 200 nm gold layer on a 20 nm titanium and 20 nm palladium adhesion layer by thermal evaporation with an Edwards Auto 306 vacuum coating system at $P < 1.10^{-8}$ bar and employed as electrodes.

The gold film substrates were primed with sulfonate groups by immersion in an MPS solution for 30 min and rinsed again with deionized water. The polymer modified electrode was constructed by immersion in PAH-Os solution for 30 min, followed by thoroughly rinsing with Milli-Q water.

3.3. Electrochemical Experiments. Redox polymer modified electrodes were probed by cyclic voltammetry at 25 mV/s in solutions containing 1 mM HNO_3 (pH 3) and different $NaNO_3$ concentrations. The measurements were carried out at room temperature (25 °C) with an Autolab PGSTAT 30 potentiostat (Autolab, Ecochemie, Holland). All experiments were performed

in a purpose built three electrode Teflon cell, with an electrode exposed area of approximately 0.25 cm^2 delimited by an inert O-ring.

An Ag/AgCl 3 M KCl (0.210 V vs NHE) electrode was employed as reference electrode; a platinum gauze auxiliary electrode of large area was employed. Before thiol adsorption the electrode potential was cycled in 2 M sulfuric acid between 0.2 and 1.6 V at 0.1 V s^{-1} to check for surface contamination and electrochemically active areas were calculated from the reduction peak of gold oxide.[57]

The liquid junction potentials across the reference electrode frit were estimated using the Henderson equation[8] and used to correct the experimentally measured current potential curves.

4. Results and Discussion

4.1. Theory−Experiment Comparison. The current−potential curves in linear scan voltammetry experiments under reversible conditions can be calculated from the theory using

$$j = j_{\text{non-redox}} + j_{\text{redox}} = (C_{\text{non-redox}} + C_{\text{redox}})\upsilon \qquad (44)$$

where υ is the experimental scan rate parameter $\upsilon = dE_{eq}^{abs}/dt$. We will use hereafter the convention, which assigns positive values for the oxidation (anodic) currents.

In order to compare the predictions of the theory with the electrochemical experiments, it is necessary to relate the absolute electrode potentials with the potentials measured during the electrochemical experiments against Ag/AgCl reference electrode. On the basis of the work of Trasatti[40] on the absolute potential scale, we can write

$$E_{\text{abs}} = E_{\text{Ag/AgCl}}^{\text{abs}} + E^{\text{Ag/AgCl}} \qquad (45)$$

where $E_{\text{Ag/ACl}}^{\text{abs}}$ is the potential of the Ag/AgCl electrode in the absolute scale (−4.65 V) and $E^{\text{Ag/AgCl}}$ is a potential measured against Ag/AgCl. This equation can be used to calculate $E_{\text{Os(II)/Os(III)}}^{0,\text{abs}}$ (−4.385 V) in eq 36 from the experimental redox potential of the redox couple in solution (0.265 V vs Ag/AgCl).[27] Equation 45 has also been employed to convert the theoretical potentials back to the Ag/AgCl reference scale after solving the theory. To determine ψ^{M} from E_{eq}^{abs} using eq 38, we have used $\Phi_{e^-}^{M} = -4.7$ eV (the work function of polycrystalline gold[58,59]). The electrode potentials in the rest of this work are expressed in the Ag/AgCl reference potential scale.

It is also important to recall that eq 44 is only valid when all of the redox sites in the film are in electrical equilibrium with the metal. In other words, the experimental characteristic time must be much longer that the characteristic times for charge transfer at the film−metal interface and diffusional charge transport inside the film. We have found a constant charge for electrochemical measurements at $\upsilon < 0.1$ V/s, and thus, we performed the experiments at a lower scan rate (0.025 V/s) in order to eliminate charge transfer and transport effects.

Figure 2 shows the calculated and measured current−potential curves for two different salt concentrations. Note the almost zero peak separation in the experimental voltamperograms, indicating that the redox equilibrium is fulfilled in the entire system at each electrode potential as it is required in order to compare with the molecular theory of reversible redox process. The predicted current−potential curves reproduce most, if not all, of the experimental measurements. We have chosen two salient features of the cyclic voltammetric surface waves to demonstrate the predictive power of the theory: the peak position (E_{peak}) and the peak full width at half-height (fwhh). The comparison of these parameters in the entire range of ionic strengths is displayed in Figure 3. There is very good agreement between the predictions and the experimental observations for the entire range of salt concentrations. The predictive power of the theory enables us to look in detail at the relationship between the structure of the polymer film and the electrochemical observed behavior. In particular, how molecular variables and solution conditions affect the molecular structure of the film and its relationship to the electrochemical response.

The shift of the redox peak toward positive potentials with the decrease in the ionic strength is attributed to the presence of the Donnan interfacial potential[9] due to the positive electrostatic charges of the polymer that exclude ions of same charge from the solution. It is interesting to note that the usually called Donnan equilibrium is explicitly included in the molecular theory. However, due to the strong coupling between molecular organization and the (local) electrostatic potential, changes in the Donnan equilibrium are associated with changes in the distribution of molecular species, some of which we describe in detail below. The Donnan equation, on the other hand, makes use of an adjustable parameter (the molar concentration of polymer charged sites), whereas the theory provides the same quantities from a first principle calculation and without adjustable parameters.

The prediction of the peak broadening at low ionic strengths beyond the ideal value of 90.6 mV for a one-electron reaction[12] is very remarkable. In previous models, peak broadening has been related to repulsive interactions that result in a distribution of activity coefficients dependent on the degree of film oxidation[60] or a Gaussian distribution of formal redox potentials due to heterogeneities in the layer,[61] therefore introducing adjustable parameters obtained from the experiment. Changes in the Donnan potential due to changes in the electrostatic charge in the polymer could also lead to peak broadening in the particular case of electrodes modified by permselective redox polymers.[62] Interestingly, the molecular theory is capable of providing a microscopic picture for the distribution of lateral interactions as a function of the distance form the surface. As we will show below (see, e.g., Figures 5−8), the distribution of redox sites and other charges, as well as the electrostatic potential, is not trivial, and it is highly inhomogeneous. Moreover, a distribution of formal redox potentials results from the thermodynamic requirement of constant chemical (electrochemical) potential for all surface distances and for all of the molecular species. Thus, our theoretical treatment does not impose one or the other mechanisms for the peak broadening. Rather, we find that they are a result of a combination of the two effects coupled with changes in the molecular organization as a function of the solution ionic strength.

A second piece of experimental information that can be checked against the predictions of the theory is the film thickness. Ellipsometry provides a nonelectrochemical source to determine this quantity. The theoretically average film thickness, $\langle z \rangle$, is defined as the first moment of the volume fraction distribution of the polymers. Namely

$$\langle z \rangle = \frac{\int (\langle \phi_P(z) \rangle + \langle \phi_{Os}(z) \rangle)(z - \delta_{MPS})\, dz}{\int (\langle \phi_P(z) \rangle + \langle \phi_{Os}(z) \rangle)\, dz} \qquad (46)$$

The in situ ellipsometric thickness for a completely reduced layer on PAH-Os on Au/MPS immersed in a 0.2 M KNO_3 pH 7.3 buffer solution has been measured and reported elsewhere.[26] Under the same conditions and employing the parameters in

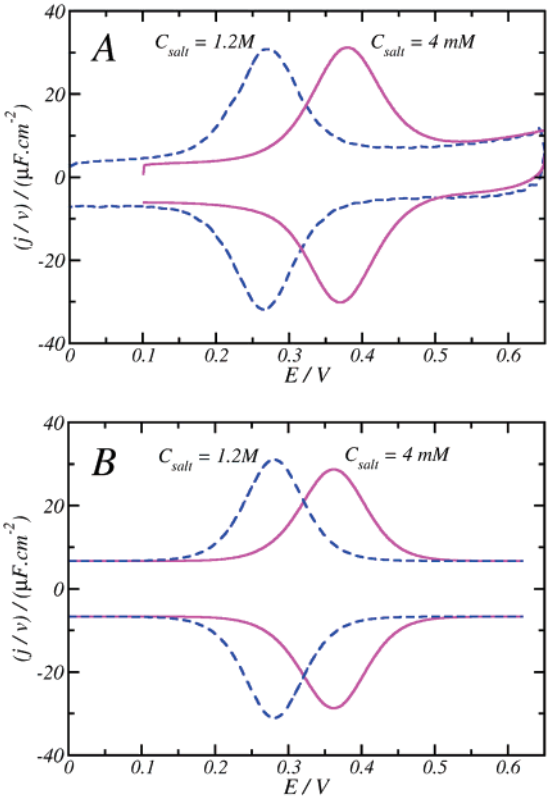

Figure 2. Comparison of experimental (A) and theoretical (B) current−potential plots measured at $\upsilon = 0.025$ V/s for a Au/MPS/PAH-Os electrode in HNO_3 1 mM (pH 3) and two different salt ($NaNO_3$) concentrations. The currents have been normalized with the scan rate and a common scale has been used in both figures.

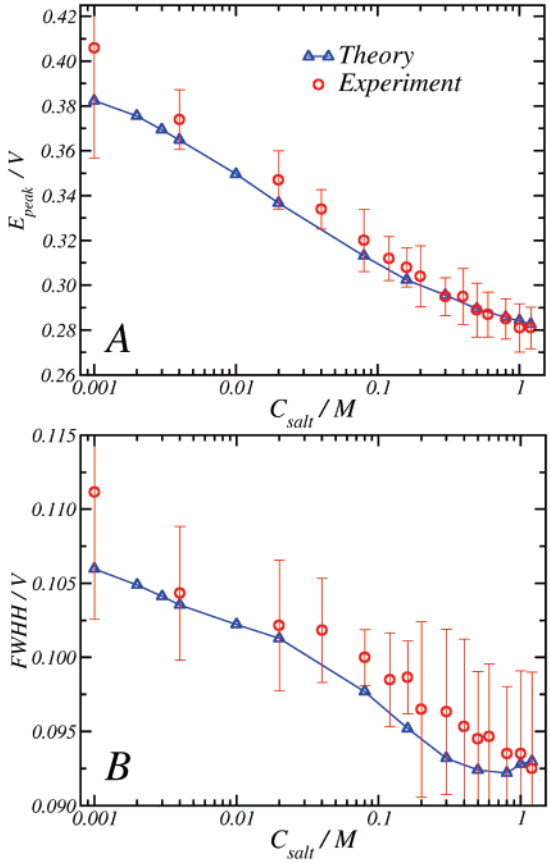

Figure 3. Plots of peak potential position (A) and peak width (B) vs salt concentration in the bulk solution determined from the experimental and theoretical redox waves in the same conditions of Figure 2. The experimental data presented is an average from the oxidation and reduction peaks obtained from three different sets of cyclic voltammetry experiments. The error bars indicate three standards deviations from the average.

section 3, the theory predicts a thickness of 1.2 nm in good agreement with the experimental value of 1.5 nm.

The ability of the theory to predict the current−potential curves and independently the film thickness strongly suggests that the structural information obtained from the theory (and the resulting electrochemical behavior) is correct. We will show next how changes in the molecular properties of the redox polyions result in rather different predictions for both the structure and current−potential curves. Thus, a proper description of the film requires a detailed molecular treatment and further, we can use the theory as a design tool for the type of molecular structure that can lead to a given electrochemical response.

4.2. Effect of the Molecular Model. The strength of the theory is in its ability to rationally design integrated electrochemical systems based on the understanding of the relationship between the properties of the system and its molecular details. This point is illustrated in Figure 4, where we show predictions for different molecular models for the polymer that differ from the PAH-Os molecular model defined in section 3.

We call good solvent molecular model a polymer that likes to be surrounded by the solvent. As explained in the Theory section, the quality of the solvent is accounted for through the strength of the vdW interaction parameter, $\chi(|z - z'|)$. In the good solvent $\chi(|z - z'|) = 0$, and therefore, the only nonelectrostatic interactions included in the system are excluded volume repulsions. This implies that the polymer molecules would like to swell as much as possible. In the PAH-Os molecular model however, solvent is considered poor and the polymer chains tend to form compact (collapsed) structures. The good solvent molecular model systematically predicts thicker films than those experimentally observed, i.e., $\langle z \rangle = 5.8$ nm vs an ellipsometric thickness of 1.5 nm measured in ref 26. The peak position predicted by this model, as shown in Figure 4A, differs also appreciably with that of the PAH-Os model and, thus, with the experimental observations. Differences in the peak widths between the two qualities of solvent are not as evident.

The second example that we show to demonstrate the coupling between molecular structure, film organization, and electrochemical behavior corresponds to a polymer in which the redox site is assumed to be smaller that in PAH-Os. The small redox site molecular model is modeled with redox sites whose radiuses are 4.6 Å (estimated for example for amino ruthenium complexes[63]). This radius is to be compared with 7.5 Å estimated for the pyridine−bipyridine osmium complex used in the PAH-Os model. Figure 4, panels A and B, shows the remarkable influence of the redox sites size on the peak parameters. In particular note the slope of the peak potential position vs salt concentration, for low C_{salt}, which is close to 22 mV per order of magnitude in salt concentration. This is much less than the 60 mV predicted by the Donnan equation[27] for a one-electron anion-permselective process. The different molecular organization of the different molecular models is described below. At this point, it is important to emphasize that the treatment of the polymer film of interest with the Donnan equation is inadequate due to the finite thickness of the film.[64,65] On the other hand, our theoretical treatment can be thought as a generalized Poisson−Boltzmann method, see section 2. Therefore, the predictions from the theory provide the full

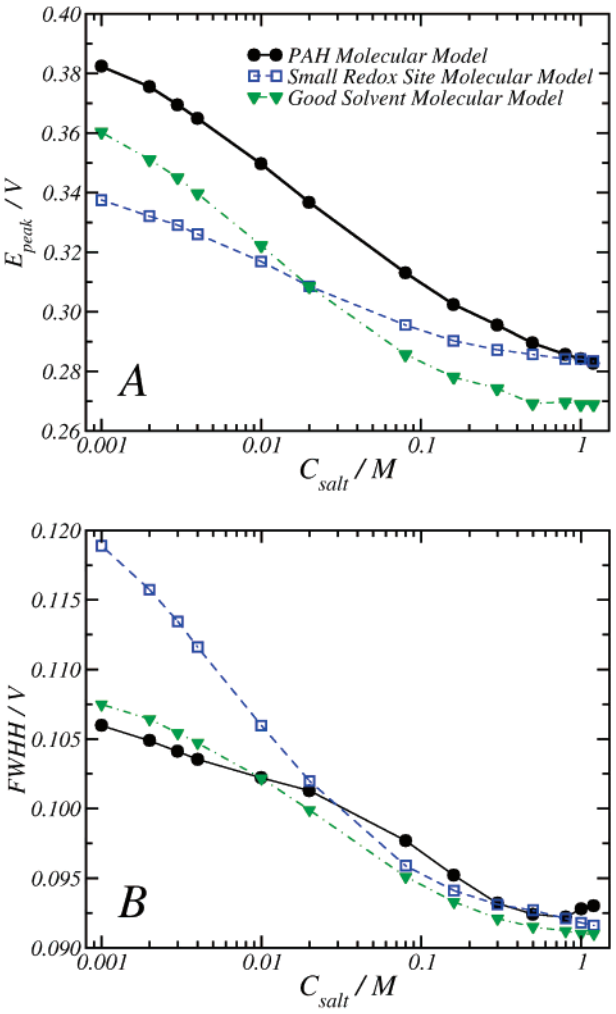

Figure 4. Plots of peak potential position (A) and peak width (B) vs salt concentration in the bulk solution calculated for different molecular models described in section 4.2 using pH = 3.

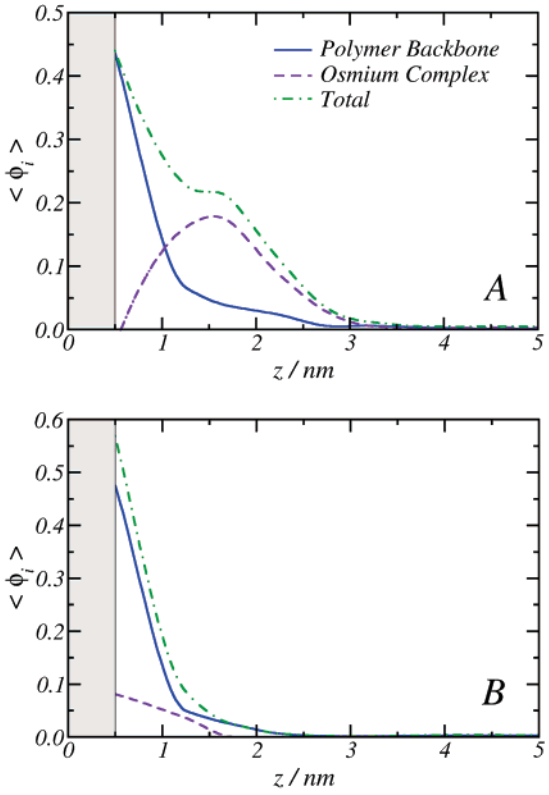

Figure 5. Theoretical volume fraction profiles for the polymer backbone (full line), the redox sites (dashed line), and the whole redox polymer (dot-dashed line) obtained for the PAH-Os molecular model described in section 3 (A), and the small redox site molecular model described in section 4.2 (B). The calculations were performed at $E = E^0_{Os(II)/Os(III)}$ using $C_{salt} = 0.1$ M and pH = 3. The shaded region ($z <$ 0.5 nm) is occupied by the thiol layer.

variation of the electrostatic and redox potentials as a function of the distance from the surface.

4.3. Structure of the Electrode/Polymer/Solution Interface. We shall discuss now the molecular insights of the electrode/polymer/solution interface obtained from the theory. Figure 5 shows the volume fraction for the polymer backbone, the osmium complex, and the whole redox polymer as a function of the distance form the surface, z, at $E = E^0_{Os(II)/Os(III)}$. Figure 5A corresponds to the experimentally studied system, i.e., PAH-Os model. The distribution of the polymer segments is found mostly close to the surface; however, the profiles do not completely decay to zero until approximately 12 nm. This indicates a strong adsorption of most of the allyl-amine segments of the polymer on the thiol layer and a small population of extended dangling tails protruding into the solution. Another interesting feature in the density profiles is the exclusion of the bulky and rigid redox sites from the surface by the smaller and more flexible polymeric chains. This result is relevant to the distance-dependent electron-transfer rate. For instance, the heterogeneous electron-transfer rate constant at the polymer/electrode interface measured by electrochemical impedance spectroscopy has been found to be much less than the rate constant for a soluble osmium complex.[26] The kinetics of electron transfer are beyond the scope of the present work. However, the predictions of the MT can be used to formulate a theory for the kinetics of electron transfer with the proper incorporation of the distribution of redox sites.

Figure 4 has shown that the electrochemical response of the polymer-modified electrodes depends dramatically on the molecular nature of the polymers. To show the link between that response and the molecular structure of the film, Figure 5B displays the volume fraction distribution for the small redox site molecular model. In this case, the redox sites are not excluded from the surface due to the much smaller size as compared to the osmium pyridine−bipyridine complex (see Figure 5A). The presence of the small redox groups in the vicinity of the negatively charged thiols surface decreases the local electrostatic potential sensed by these sites and gives rise to the low slope observed in Figure 4A. The effect of the redox site size underlines the strong coupling that exists between the structure and the electrochemical response the polymer film. This coupling emphasizes the need for a molecular approach to describe the complexity of the polymer modified electrodes.

A more detailed manifestation of the complexity of the system can be seen by looking at the electrostatic potential as a function of the distance from the surface. This is displayed in Figure 6 together with the total polymer volume fraction. The electrostatic potential starts positive on the surface as a result of the applied potential on the metal. It has a sharp decrease to negative values within the thiol layer due to the presence of the negatively charged sulfonate end groups of the thiol. There is an increase of the potential to positive values in the region of the adsorbed polymer. The maximum of the potential coincides with the inflection point in the volume fraction of the polymer profile, which corresponds to the maximum in the distribution of the osmium groups. The maximum is followed by a long tail of positive potential that reflects the dangling polymer tails.

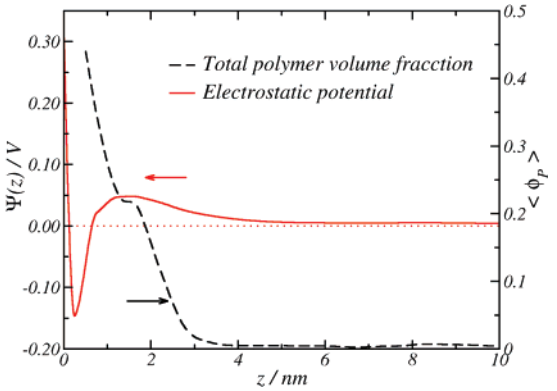

Figure 6. Electrostatic potential as a function of the distance from the metal (full line, left axis) calculated for a Au/MPS/PAH-Os electrode with the PAH-Os molecular model for the same conditions as Figure 5. The total polymer volume fraction profile is shown by the dashed line (left axis).

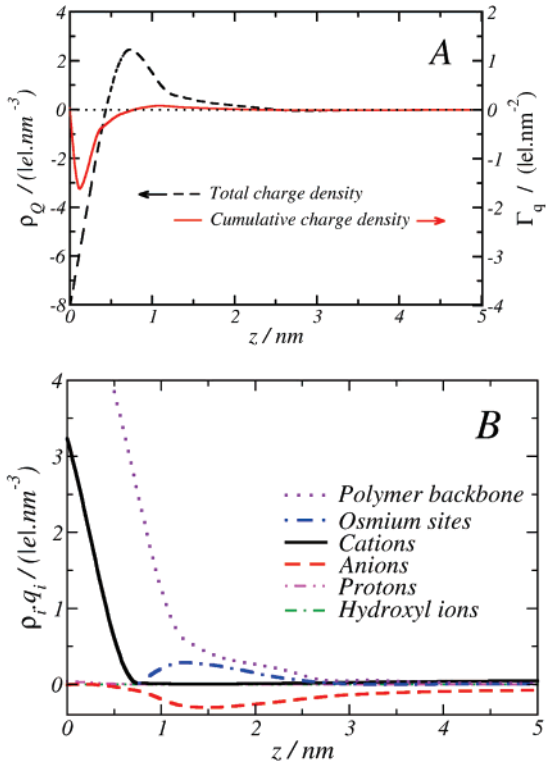

Figure 7. A. Total charge density (dashed line, left axis), eq 15, and cumulative charge density (full line, right axis), eq 47, as a function of the distance from the electrode. B. Charge density profile for each of the charged molecular species considered by the theory. The calculations were performed using the PAH-Os Molecular Model for the conditions of Figure 5. For a better visualization of the densities of protons see the inset in Figure 8.

Interestingly, the decay length of the potential is not related to the Debye length, which in this case is of the order of 1 nm, but rather it is the distribution of charges driven by the molecular organization of the polymer that controls the electrostatic potential.

The complete distribution of charges, $\langle \rho_q(z) \rangle$, and the contribution from each molecular species are shown in Figure 7. The total charge at each distance from the surface reflects the same trends described with the electrostatic potential. The interesting result shown in Figure 7A is the cumulative charge density defined by

$$\Gamma_q(z) = \sigma_M + \int_0^z \langle \rho_q(z') \rangle \, dz' \qquad (47)$$

where σ_M is the charge density on the metal surface. The cumulative charge density represents the total (integrated) charged from the metal surface up to the distance z. As can be seen from the figure, the polymer layer exhibits the effect of charge reversal. Namely, there is a distance from the surface where the total charge becomes compensated, and at further distances, the effective surface charge changes sign. This is important because it shows the position where a second layer of polymers or proteins is expected to adsorb in the formation of layer by layer assembly.[66] The magnitude of charge reversal is not very large in the case shown. Moreover, we do not attempt to quantify the optimal conditions for this effect.[67] The important result is how the charge reversal arises from the molecular organization of the film and the distribution of the different charged components. This is explicitly shown in Figure 7B.

There is a large adsorption of cations inside the thiol layer to compensate for the large charge arising from the negatively charged sulfonate groups from the thiol. There is a further large adsorption of positive charges arising from both the polymer and the Os. Within this region, 0.5 nm $< z <$ 2.5 nm, there is also an adsorption of anions to reduce the possibility of very large local positive charge that would result in strong electrostatic repulsion. The number of polyions, with their associated Os groups, is large enough to compensate for all of the negative charge at about $z = 2$ nm resulting in the charge reversal. The positive charge is maintained up to $z = 4$ nm, where all of the charge is compensated for again by the anions, and the cumulative charge is zero from there to the bulk solution.

A very insightful result obtained from Figure 7 is that the charges are not localized in well-defined surfaces but are distributed in a way to optimize electrostatic interactions, molecular packing effects, and entropic effects, e.g., counterion release. It is well-known that in polymer layers where charge regulation is possible, for example by acid−base equilibrium, the degree of dissociation is highly inhomogeneous.[25,36,68,69] In the present case, and with particular relevance to the electrochemical behavior, the question that arises is what is the distribution of oxidized (and reduced) groups along the adsorbed polymer layer.

Figure 8 displays the total distribution of osmium groups together with the fraction of the oxidized sites. According to the applied potential in the case shown, one would expect in a bulk solution of free osmium complexes to have half of the moieties oxidized and half of them reduced. However, the predictions of the theory show that this is not at all the case in the film, and there is a rather large variation of the fraction of oxidized groups depending on the location relative to the electrode surface. This implies the existence of a z-dependent distribution of redox sites with different formal redox potentials due to local environment effects, which result in peak broadening.

The fraction of oxidized states is a nonmonotonic function of the distance from the electrode. The quantitative effect is very large, with the minimum in the fraction of oxidized group reaching 0.15. This value is a factor of 3 smaller that what would be expected from the free osmium in solution at $E = E^0_{Os(II)/Os(III)}$ in the absence of local environment effects, i.e., $f^{bulk}_{Os} = 0.5$. The understanding of the source of the effect can be traced to eq 34, where the fraction of oxidized groups is found to be related to the electrode and standard potentials and to the local electrostatic potential. However, as shown in the derivation of the theory, the electrostatic potential is strongly

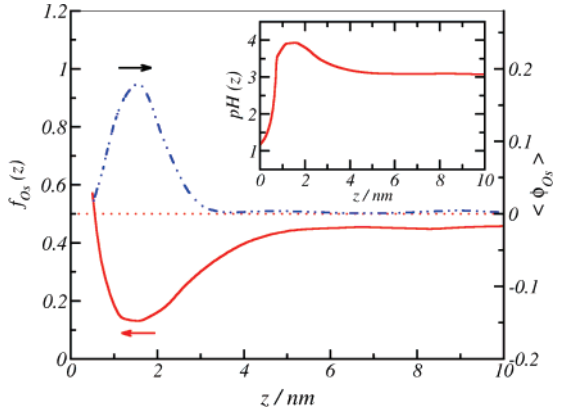

Figure 8. Fraction of oxidized redox sites (solid line, left axis) and osmium site volume fraction (dashed line, right axis) as a function of the distance from the electrode at $E = E^0_{Os(II)/Os(III)}$. Inset: local pH vs distance from the electrode. The PAH-Os molecular model and the conditions of Figure 5 were used in the calculations.

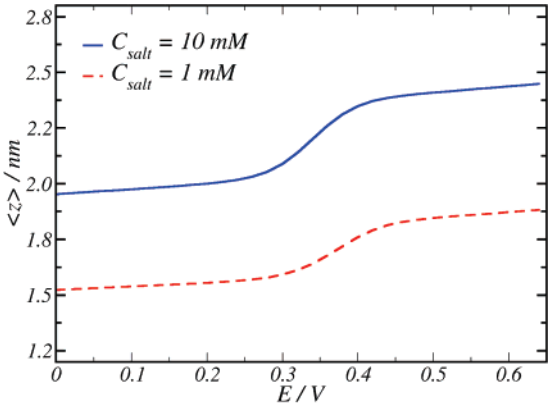

Figure 9. Theoretical predicted thickness-potential curves calculated for two different salt concentrations at pH = 3.

coupled to the interactions, and therefore, it is the result of local and nonlocal electrostatic and packing effects. Namely, the highly nonmonotonic electrostatic potential presented in Figure 6 is responsible for the variations of $f_{Os}(z)$, but as discussed above the shape of the electrostatic potential in these complex systems depends on the packing and the distribution of all the charged (and uncharged) molecules.

Another manifestation of the non-trivial distribution of molecular species in the film is seen in the local pH, defined by $pH(z) = -\log[H^+(z)]$. This is shown in the inset of Figure 8. Note that the proton distribution is also shown in Figure 7B; however, its distance dependence cannot be observed on the scale of that plot. The thin film is very acidic in the thiol region due to the presence of the sulfonate groups there. In the region rich in osmium and amino groups, there is a large repulsion to the protons and, therefore, a higher pH value as compared to the bulk value. The shape of the local pH profile follows that of the fraction of oxidized redox sites. The smaller the fraction of oxidized osmium sites, the smaller the concentration of protons. Interestingly, the changes in local pH from the metal to the maximal pH are very dramatic, reflecting changes in the local concentration of protons larger than 2 orders of magnitudes within 1 nm. This large gradient in pH may have potential applications in the design of sensors and they have to be taken into account in understanding chemical reactivity in nanoconfined environments. Local variations of pH have been observed experimentally in LbL films by v. Klitzing and Möwald.[70]

4.4. Theoretical Description of the Electrochemical Process. The swelling of polymer films during redox switching and the resulting changes in film volume upon changes in the oxidation state are well established in polymer electrochemistry.[7] The electrochemical driven swelling has been studied in layer by layer[53,71] polymer modified electrodes with PAH-Os by electrochemical quartz crystal microbalance (EQCM) and in situ ellipsometry.

The molecular theory can predict the redox-driven swelling; in order to show this, we have plotted the calculated average film thickness as a function of the applied electrode potential in Figure 9 for two different solution ionic strengths. The shape of the thickness−potential curves and the inflection point at $E = E_{peak}$ is in very good qualitative agreement with previous ellipsometric measurements in PAH-Os/poly(vinyl-sulfonate) multilayers.[71] Although a direct comparison of these experimental observations is not possible since the theory has been applied to a single PAH-Os layer, the driving force for the swelling is the same in both cases, and it can be traced to the fact that the increase in the electrostatic charge increases the electrostatic repulsions. The system relaxes in different ways: by swelling, by the uptake of counterions, and by charge regulation (protonation effects). The results in Figure 9 show contributions from all three effects.

During the electrochemical oxidation process, the flux of electrons into/from the polymeric film requires a simultaneous exchange of mobile ions with the bulk solution in order to sustain the system electroneutrality. As an example, during Os(II) oxidation, anion uptake or cation release are expected to occur. Although it is not possible to study the ion exchange mechanism using only electrochemical techniques, there are several in situ methods, such as EQCM and probe beam deflection (PBD), which can probe the ionic fluxes close to the electrode surface. The molecular theory allows the straightforward calculation of the individual ionic contributions to the non-redox and redox capacities[18] and therefore to the ionic fluxes under electrochemical reversible conditions. Following the same ideas used in the derivation of eqs 39, 41, and 44, the individual normalized ionic current for each ion is determined from the potential dependence of its surface excess. Namely

$$\frac{j_i}{\upsilon} = -q_i F \frac{\partial \int (\rho_i(z) - \rho_i^{bulk})\, dz}{\partial E_{eq}^{abs}} \tag{48}$$

In the particular case when $i = H^+$, eq 48 should be modified to include the protons associated with the polymer and MPS to lead to

$$\frac{j_{H^+}}{\upsilon} = -q_{H^+} F \left(\frac{\partial \int (\rho_{H^+}(z) - \rho_{H^+}^{bulk})\, dz}{\partial E_{eq}^{abs}} + \frac{\partial \int f_c(z)\langle n_P(z)\rangle\, dz}{\partial E_{eq}^{abs}} + \frac{\partial \int [(1 - f_{c,MPS}(z))\langle n_{MPS}(z)\rangle]\, dz}{\partial E_{eq}^{abs}} \right) \tag{49}$$

Figure 10 exhibits the scan rate normalized ionic currents during film oxidation under permselectivity conditions (low ionic strength). The concentrations of protons and hydroxyls ions are coupled by the water self-dissociation equilibrium, and therefore, their ionic fluxes cannot be addressed individually but as a combined current. It is also worthwhile to note that the sum of all ionic currents is equal to the total electronic current obtained by combination of its redox and non-redox components.

For either totally oxidized or totally reduced redox polymers, i.e., $E \leq 0.10$ or $E \geq 0.55$ V in Figure 10, we find that cations

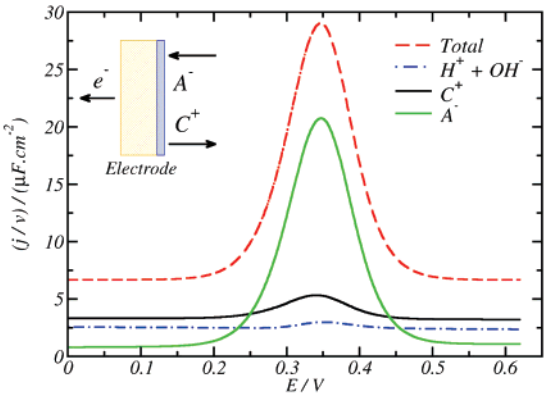

Figure 10. Scan rate normalized ionic currents vs electrode potential calculated with eqs 48 and 49 and the PAH-Os molecular model for C_{salt} = 10 mM and pH = 3. Inset: Scheme showing the directions of ionic and electronic currents.

are responsible for non-redox charging. The compensation of redox charge, on the other hand, is achieved mainly by the anions and to a lesser extent by the cations. Thus, the theory predicts the exchange of both anions and cations, which is consistent with previous PBD experiments in PAH-Os capped PAH-Os/PVS multilayers.[72,73]

To the best of our knowledge, this is the first theoretical prediction of volume change and ionic contribution to the charge compensation in chemically modified electrodes.

5. Conclusions

We have applied a molecular theory to study the structure and thermodynamic properties of a monolayer of redox polyelectrolyte adsorbed on a mercapto propane sulfonate thiolated gold electrode in contact with an aqueous electrolyte. The theory explicitly incorporates the size, shape, conformations, charge, and charge distribution of all of the molecular species. Through a free energy formulation, we include conformational dependent electrostatic, van der Waals, adsorption and excluded volume interactions, as well as the chemical equilibrium for the different acid−base and redox groups. The approximations used in the derivation of the theory as well as its limitations have been extensively discussed elsewhere.[34−36]

The theory predicts the current−potential curves under reversible conditions, the dependence of the peak potential position and the peak width with the electrolyte concentration, and the film thickness and its dependence on the electrolyte concentration and the electrode potential. Excellent agreement of these predictions with the experimental results for the Au/MPS/PAH-Os system has been found for different experimental conditions without the use of any free adjustable parameter. It is important to emphasize that the theoretical approach presented here does not separate double layer charging and redox pseudocapacitive currents as independent quantities, as is usually done in most electrochemical literature. The molecular theory accounts for the total flow of charge, including any possible cross interaction, and enables the understanding of the relationship between the current−potential curves observed and the molecular structure of the film.

The theory predicts the distribution profiles of all molecular species in the direction normal to the electrode surface. The resulting profiles show total compensation of charge at some distance from the electrode surface and charge overcompensation by the polyelectrolyte tails protruding in the external electrolyte. This prediction is consistent with previous experimental findings and is the driving force for the formation of polyelectrolyte multilayers.

The distribution of the allyl-amine segments forming the polymer backbone is found to be mostly that of a tightly adsorbed layer with most of the segments in the close vicinity of the surface with a few long dangling tails protruding into the solution. The osmium complex concentration fraction profile exhibits a maximum at a distance from the electrode surface as a result of the bulky size of the osmium pyridine-bipyridine moiety. This result is relevant to understand the distance-dependent electron-transfer process with the metal electrode. The distribution of the formal redox potentials in the direction normal to the electrode predicted by the theory is the result of the complex interplay between the electrostatic potential, the molecular packing, and the distribution of charged species. The existence of a nonuniform formal redox potential is consistent with the concepts of Anson et al.[60] and Albery et al.[61] to explain the peak broadening.

The comparisons with the experimental observations have been carried out for a model polymer that is in a poor solvent environment. This condition leads to the tendency of the polymer to collapse. On the other hand, the strong electrostatic repulsions tend to swell the polymer as much as possible. Overall, the compromise results in a polymer in a mildly poor solvent. The thickness of the predicted film is in line with experimental observations based on ellipsometry. We have shown that the theory applied to the case of a good solvent predicts a much thicker layer than the experimental observations and the electrochemical peak positions are poorly predicted.

The size of the redox sites has a dramatic influence on the structure and current potential curves of the polymer film. This demonstrates the important coupling that exists between molecular organization and electrochemical response, and it furthers points out to the need to describe the polymer layer at the molecular level.

The predictive capacity of the molecular theory presented here brings the possibility of a rational design of chemically modified electrodes tailored to precise properties. Furthermore, the theory allows the determination of the conditions where approximate (analytical) models are valid. We are currently extending the molecular approach to study LbL deposition in polyelectrolytes and proteins. Moreover, we are coupling the structural features predicted by the theory to the kinetics of electron transfer.

Acknowledgment. E.J.C. and M.T. acknowledge financial support from CONICET (Argentina), the University of Buenos Aires, and ANPCyT (BID 1728 OC-AR PICT 2003 No. 06-17170). M.T. has a cooperative CONICET-FUDETEC industrial research grant. E.J.C. is a permanent research staff of CONICET. I.S. acknowledges the financial support from the National Science Foundation of the United States CTS-0338377 and NIRT-0403903 and the Raices-Milstein Program of the Argentine Secretary for Science and Technology (SETPCyT).

Supporting Information Available: A detailed description of the numerical methods used to solve the molecular theory; the chain model and generation method and the effect of the chain length and complete ref 69. This material is available free of charge via the Internet at http://pubs.acs.org.

References and Notes

(1) Moses, P. R.; Wier, L.; Murray, R. W. *Anal. Chem.* **1975**, *47*, 1882.
(2) Murray, R. W. *Acc. Chem. Res.* **1980**, *13*, 135.
(3) Murray, R. W. Chemically Modified Electrodes. In *Electroanalytical Chemistry*; Bard, A. J., Ed.; Marcel Dekker: New York, 1984; Vol. 13; p 191.

(4) Murray, R. W. Introduction to Molecularly Designed Electrode Surfaces. In *Molecular Design of Electrode Surfaces*; Murray, R. W., Ed.; John Wiley and Sons, Inc.: New York, 1992.
(5) Bard, A. J. *Integrated Chemical Systems. A Chemical Approach to Nanotechnology*; John Wiley & Sons: New York, 1994; Vol. 1.
(6) Hodak, J.; Etchenique, R.; Calvo, E. J.; Singhal, K.; Bartlett, P. N. *Langmuir* **1997**, *13*, 2708.
(7) Lyons, M. E. G. *Electroactive Polymer Electrochemistry*; Plenum Press: New York, 1994; Vol. 1.
(8) Bard, A. J.; Faulkner, L. R. *Electrochemical Methods: Fundamentals and Applications*, 2nd. ed.; John Wiley & Sons: New York, 2001.
(9) Doblhofer, K.; Vorotyntsev, M. Fundamentals. In *Electroactive Polymer Electrochemistry*.; Lyons, M. E. G., Ed.; Plenum: New York, 1994; p 375.
(10) Naegeli, R.; Redepenning, J.; Anson, F. C. *J. Phys. Chem.* **1986**, *90*, 6227.
(11) Redepenning, J.; Anson, F. C. *J. Phys. Chem.* **1987**, *91*, 4549.
(12) Laviron, E. *J. Electroanal. Chem.* **1979**, *100*, 263.
(13) Andrieux, C. P.; Savéant, J. M. *J. Phys. Chem.* **1988**, *92*, 6761.
(14) Anson, F. C.; Blauch, D. N.; Savéant, J.-M.; Shu, C.-F. *J. Am. Chem. Soc.* **1991**, *113*, 1922.
(15) Blauch, D. N.; Savéant, J. M. *J. Phys. Chem.* **1993**, *97*, 6444.
(16) Savéant, J. M. *J. Phys. Chem.* **1988**, *92*, 4526.
(17) Laviron, E. *J. Electroanal. Chem* **1980**, *112*, 1.
(18) Chidsey, C. E. D.; Murray, R. W. *J. Phys. Chem.* **1986**, *90*, 1479.
(19) Bowden, E. F.; Dautartas, M. F.; Evans, J. F. *J. Electroanal. Chem.* **1987**, *219*, 49.
(20) Dautartas, M. F.; Bowden, E. F.; Evans, J. F. *J. Electroanal. Chem.* **1987**, *219*, 71.
(21) Bowden, E. F.; Dautartas, M. F.; Evans, J. F. *J. Electroanal. Chem. Interfacial Electrochem.* **1987**, *J219*, 91.
(22) Posadas, D.; Florit, M. I. *J. Phys. Chem. B* **2004**, *108*, 15470.
(23) Lizarraga, L.; Andrade, E. M.; Florit, M. I.; Molina, F. V. *J. Phys. Chem. B* **2005**, *109*, 18815.
(24) Hill, T. L. *An Introduction to Statistical Thermodynamics*; Dover Publications: New York, 1986.
(25) Netz, R. R.; Andelman, D. *Phys. Rep.* **2003**, *380*, 1.
(26) Tagliazucchi, M.; Calvo, E. J. *J. Electroanal. Chem.* **2007**, *599*, 249.
(27) Calvo, E. J.; Wolosiuk, A. *J. Am. Chem. Soc.* **2002**, *124*, 8490.
(28) Calvo, E. J.; Danilowicz, C.; Wolosiuk, A. *J. Am. Chem. Soc.* **2002**, *124*, 2452.
(29) Calvo, E. J.; Etchenique, R.; Pietrasanta, L.; Wolosiuk, A. *Anal. Chem.* **2001**, *73*, 1161.
(30) Flexer, V.; Forzani, E. S.; Calvo, E. J.; Luduena, S. J.; Pietrasanta, L. I. *Anal. Chem.* **2006**, *78*, 399.
(31) Calvo, E. J.; Danilowicz, C. B.; Wolosiuk, A. *Phys. Chem. Chem. Phys.* **2005**, *7*, 1800.
(32) Calvo, E. J.; Wolosiuk, A. *ChemPhysChem* **2004**, *5*, 235.
(33) By reversible conditions, we mean the equilibrium behavior of the electrodes; the generalization to study the kinetics of the electrochemical process is left to future work.
(34) Szleifer, I.; Carignano, M. A. *Adv. Chem. Phys.* **1996**, *96*, 165.
(35) Szleifer, I.; Carignano, M. A. *Macromol. Rapid Commun.* **2000**, *21*, 423.
(36) Nap, R.; Gong, P.; Szleifer, I. *J. Polym. Sci. Part B* **2006**, *44*, 2638.
(37) Wu, T.; Genzer, J.; Gong, P.; Szleifer, I.; Vlcek, P.; Subr, V. Behavior of surface-anchored poly(acrylic acid) brushes with grafting density gradients on solid substrates In *Polymer Brushes*; Brittain, B., Advincula, R., Caster, K., Eds.; Wiley & Sons: New York, 2004; p 287.
(38) McPherson, T.; Kidane, A.; Szleifer, I.; Park, K. *Langmuir* **1998**, *14*, 176.
(39) Satulovsky, J.; Carignano, M. A.; Szleifer, I. *Proc. Natl. Acad. Sci.* **2000**, *97*, 9037.
(40) Trasatti, S. *Pure Appl. Chem.* **1986**, *58*, 956.
(41) de Gennes, P. G. *Scaling Concepts in Polymer Physics*; Cornell University Press: Ithaca, NY, 1991.
(42) Flory, P. J. *Principles of Polymer Chemistry*; Cornell University Press: Ithaca, NY, 1953.
(43) Carignano, M. A.; Szleifer, I. *J. Chem. Phys.* **1994**, *100*, 3210.
(44) Croze, O.; Cates, M. *Langmuir* **2005**, *21*, 5627.
(45) Schwinger, J.; DeRaad, L. J.; Milton, K.; Tsai, W.-Y. *Classical Electrodynamics*; Persus Books: Reading, MA, 1998.
(46) Llano, J.; Eriksson, L. A. *J. Chem. Phys.* **2002**, *117*, 10193.
(47) Israelachvili, J. *Intermolecular and Surface Forces*; Academic Press: San Diego, CA, 1992.
(48) Mokrani, C.; Fatisson, J.; Guérente, L.; Labbé, P. *Langmuir* **2005**, *21*, 4400.
(49) Love, J. C.; Estroff, L. A.; Kriebel, J. K.; Nuzzo, R. G.; Whitesides, G. M. *Chem. Rev.* **2005**, *105*, 1103.
(50) Ninham, B. W.; Parsegian, V. A. *J. Theor. Biol.* **1971**, *31*, 405.
(51) Tagliazucchi, M.; Williams, F.; Calvo, E. J. *J. Phys. Chem. B* **2007**, *111*, 8105.
(52) Szleifer, I.; Brinke, G. t. *J. Chem. Phys.* **1996**, *104*, 6343.
(53) Forzani, E. S.; Pérez, M. A.; Teijelo, M. L.; Calvo, E. J. *Langmuir* **2002**, *18*, 9867.
(54) Messina, R. *Macromolecules* **2004**, *37*, 621.
(55) Carrillo, J.-M. Y.; Dobrynin, A. V. *Langmuir* **2007**, *23*, 2472.
(56) Danilowicz, C.; Corton, E.; Battaglini, F. *J. Electroanal. Chem.* **1998**, *445*, 89.
(57) Finklea, H. O.; Snider, D. A.; Fedyk, J. *Langmuir* **1990**, *6*, 371.
(58) Trassati, S. *J. Electroanal. Chem.* **1974**, *54*, 19.
(59) This is an approximation since it is known that the potential of zero charge of polycristalline gold (which depends on its work function) varies upon thiol adsorption. For further details, see: Iwami, Y., Hobara, D., Yamamoto, M., Kakiuchi, T. *J. Electroanal. Chem.* **2004**, 564, 77−83 and references therein.
(60) Brown, A. P.; Anson, F. C. *Anal. Chem.* **1977**, *49*, 1589.
(61) Albery, W. J.; Boutelle, M. G.; Colby, P. J.; Hillman, A. R. *J. Electroanal. Chem.* **1982**, *133*, 135.
(62) Redepenning, J.; Miller, B. R.; Burham, S. *Anal. Chem.* **1994**, *66*, 1560.
(63) Calvo, E. J.; Etchenique, R.; Danilowicz, C.; Diaz, L. *Anal. Chem.* **1996**, *68*, 4186.
(64) Ohshima, H.; Ohki, S. *Biophys. J.* **1985**, *47*, 673.
(65) Garcia-Morales, V.; Cervera, J.; Manzanares, J. A. *J. Electroanal. Chem.* **2007**, *599*, 203.
(66) Castelnovo, M.; Joanny, J.-F. *Langmuir* **2000**, *2000*, 7524.
(67) Solis, F. J.; Olvera de la Cruz, M. *J. Chem. Phys.* **1999**, *110*, 11517.
(68) Israëls, R.; Leermakers, F.; Fleer, G. J.; Zhulina, E. B. *Macromolecules* **1994**, *27*, 3249.
(69) Rühe, J.; et al. *Adv. Polym. Sci.* **2004**, *165*, 79−150.
(70) v.Klitzing, R.; Möwald, H. *Langmuir* **1995**, *11*, 3554.
(71) Tagliazucchi, M.; Grumelli, D.; Bonazzola, C.; Calvo, E. J. *J. Nanosci. Nanotechnol.* **2006**, *6*, 1731.
(72) Grumelli, D. E.; Garay, F.; Barbero, C. A.; Calvo, E. J. *J. Phys. Chem. B* **2006**, *110*, 15345.
(73) Grumelli, D. E.; Wolosiuk, A.; Forzani, E.; Planes, G. A.; Barbero, C.; Calvo, E. J. *Chem. Commun.* **2003**, *9*, 3014.